energies

Article

Investigation of Pulverized Biomass and Coal Char Emissivity

Lukas Pörtner [1,*], Ying Gu [1,2] and Martin Schiemann [1]

[1] Energy Plant Technology, Ruhr-University Bochum, 44801 Bochum, Germany; Guying@zjou.edu.cn (Y.G.); Schiemann@leat.rub.de (M.S.)
[2] Naval Architecture and Ocean Engineering, Zhejiang Ocean University, Zhoushan 316022, China
* Correspondence: Poertner@leat.rub.de; Tel.:+49-0234-32-27280

Received: 30 June 2020; Accepted: 2 September 2020; Published: 5 September 2020

Abstract: Current work presents an optical setup, its calibration and reference process and the first results from single particle emissivity measurements of pulverized biomass and coal fuel particles. In contrast to earlier attempts, the setup offers the possibility of emissivity measurements during the whole particle burn-off. A laser ignites a single particle, placed in the center of the setup. Two photomultipliers observe the emitted particle radiation in the visible range (550 nm and 700 nm) for temperature calculation, using two-color pyrometry. An InSb-detector records the emitted particle radiation between 2.4 µm and 5.5 µm, which is later used to calculate particle emissivity in this range. The conclusion of multiple particle measurements lead to decreasing particle emissivity with increasing temperature. For coal particles the emissivity decreases from 0.45 at 2300 K to 0.03 at 3400 K. Biomass char shows a similar trend with a decrease from 0.18 (2100 K) to 0.03 (2900 K).

Keywords: biomass; pulverized fuel; two-color pyrometry; emissivity

1. Introduction

The optical properties of fuel particles are of decisive importance for radiative heat transfer in pulverized fuel combustion systems [1,2]. These particle properties include the emission of thermal radiation during the burnout process and the particle/radiation interaction involving the absorption and scattering effects at the particle surface.

In order to reduce pollution and climate change, firing alternatives to expensive coal power plants are gaining popularity. One interesting approach could be co-firing of coal and renewable biomass fuels [3]. Therefore, simulations of such systems need the crucial knowledge of the fuel properties. Emissivity especially has a large impact on the calculations of heat transfer in a combustion system [4], burning kinetics [5–7] and pyrolysis [8,9]. Literature data on pulverized coal emissivity are available to a small extent [10], whereas data on biomass are rarely available.

In the recent past, Graeser et al. [11] and Schiemann et al. [12] achieved significant progress. They measured temperature-dependent emissivity of burning coal char in two different spectral ranges. A flat flame burner provided them a burning particle streak, typical for pulverized fuel combustion systems. Two photomultipliers measured the particle temperature by two-color pyrometry. A fiber spectrometer (0.85–2.50 µm) and an InSb-detector (2.4–5.0 µm) collected the emitted infrared particle radiation [10,13]. Using the particle diameter and the temperature derived by ratio pyrometry, they calculated emissivity. Due to their measurement method, the data of each measurement are just a snapshot of a short phase during the particle burn-off, caused by the fixed optical setup. This "inflight" measurement does not offer information on the complete particle history. Therefore, the current work presents the first results gained from a newly designed setup observing burning particles during their whole burn-off process. This involves the setup, the calibration and calculation methods and first results gained from experiments with nutshell particles sized 200–450 µm and coal particles sized 160–200 µm.

2. Materials and Setup

The observed pulverized fuels in this work are walnut shell and Colombian bituminous coal particles with a size distribution of 200–450 µm for the nutshell and 160–200 µm for the coal particles. An elementary analysis of the two different fuels provides the parameters listed in Table 1.

Table 1. Proxymate and ultimate analysis of the used nutshell particles.

Proxymate analysis (wt%, Dry)	Coal	Nutshell
Volatile matter	37.81	80.18
Fix carbon	56.52	18.7
Ash	5.67	1.12
Ultimate analysis (wt%, dry)		
Carbon	68.4	46.7
Hydrogen	4.9	5.9
Nitrogen	1.52	0.178

To measure a single particle's emissivity over the whole burn-off process, a newly designed setup shown in Figure 1 was developed, using the same basic measurement techniques as Graeser et al. [10,13]. The difference of the setup is that the current version is not designed to measure particles in flight but to detect thermal radiation from spatially fixed, e.g., mechanically or acoustically levitated, particles. Instead of statistical data from single particles at specific residence times in a flow reactor, the complete temporal history of a particle can now be observed in terms of temperature and thermal radiation emission.

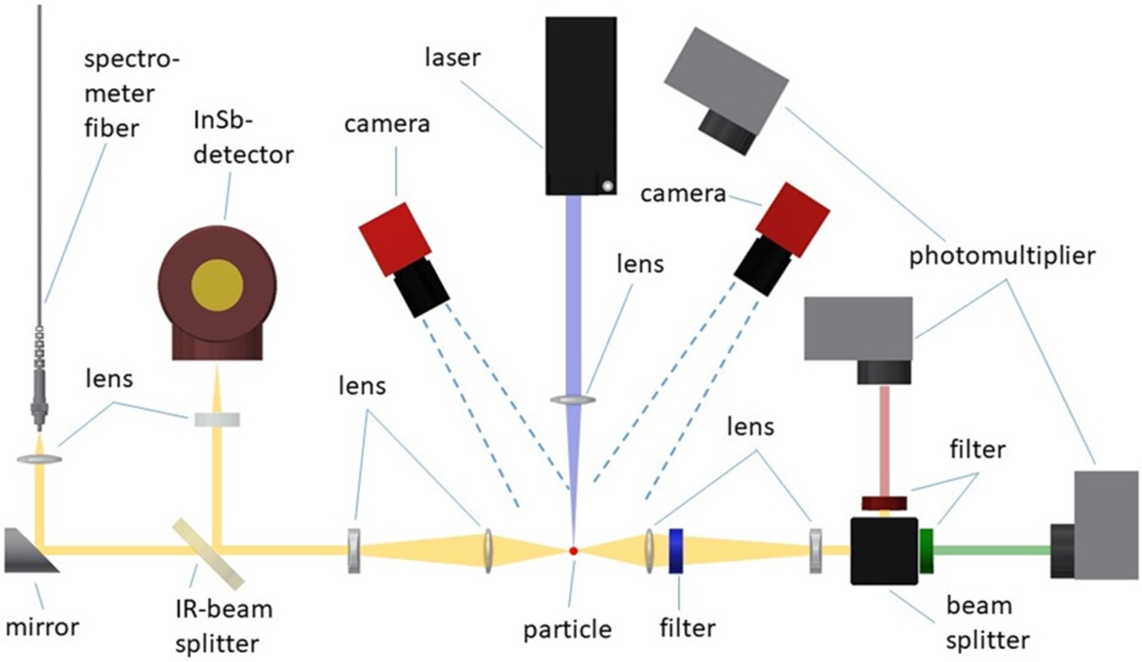

Figure 1. This figure shows a scheme of the experimental setup to investigate particle emissivity.

A focused 1.5 W diode laser (450 nm) ignites a single pulverized fuel particle in the center of a three-armed setup. Two arms detect the radial emitted light of the burning particle. The right arm of Figure 1 is responsible for the temperature measurement using two-color pyrometry at 550 and 700 nm. Here, a lens system collects the emitted particle radiation and a filter cuts off the scattered laser light. Divided into two sub beams by a 50:50 beam splitter, the light passes band-pass filters with center wavelengths of 550 and 700 nm at a FWHM (full width at half maximum) of 10 nm each. For detection, two photomultipliers (PMTs) (Hamamatsu H10723-20) are used. The left arm of the setup in Figure 1 measures the infrared radiation emitted by the particle. Again, a lens system collimates the radiation and a filter, cutting off the visible light range, protects the following detectors from damage by scattered laser radiation. A 50:50 beam-splitter divides the light into two equal sub beams. The transmitted radiation, guided and focused by a mirror and a lens, is detected by an infrared fiber-spectrometer (Hamamatsu C11118GA) in the spectral range from 0.85–2.4 µm. An InSb-detector (Hamamatsu P5968-300) records the reflected and focused sub beam from the beam-splitter in the spectral range from 2.4–5.5 µm. An additional filter in front of the InSb-detector cuts of all wavelength below 2.4 µm to get a clear separation between the detected radiation from the spectrometer and the InSb-detector. For particle positioning and adjustment routines, two cameras (Allied Vision Guppy) are implemented. Particle mounting is realized by a platinum covered steal pin. An additional photomultiplier is measuring the scattered laser radiation to monitor laser stability and reaction time.

2.1. Particle Temperature Calculation

Particle temperature is calculated by two-color pyrometry comparing the radiation intensity at 550 and 700 nm measured by the photomultipliers. Following a typical approach for two-color pyrometry described by Graeser et al. [10,11,13], the temperature is calculated by Wien's law:

$$T = c_2 \frac{\lambda_1 - \lambda_2}{\lambda_1 \lambda_2} \left(\ln\left(\kappa \left(\frac{\lambda_1}{\lambda_2} \right)^5 \right) + \ln\left(\frac{I_1}{I_2} \right) \right)^{-1} \tag{1}$$

where c_2 denotes the second radiation constant, $\lambda_1 = 550\,\text{nm}$, $\lambda_2 = 700\,\text{nm}$, I_1 is the signal intensity of λ_1 and I_2 is the signal intensity of λ_2. The calibration constant κ is individual for every measurement setup and needs to be determined from calibration measurements. Therefore, the complete arm for temperature measurements is positioned in front of a blackbody reference radiation source. At maximum blackbody temperature (T_{max} = 1973.15 K), an adjustable, water-cooled pinhole aperture at the blackbody output avoids detector saturation by reducing the output diameter. For all following temperature calibration measurements, this opening diameter stays constant. Lowering the blackbody temperature from 1973.15 to 573.15 K in steps of 10 K, three measurements with the PMTs are carried out, collecting 15,000 data points per measurement, photomultiplier and temperature. In the end, the blackbody is turned off and an additional background measurement at room temperature is performed. The averaged and background-reduced signals for each temperature are presented in Figure 2. Fitting Wien's law Equation (1) to the theoretical temperature function leads to $\kappa = 0.278\,634 \pm 4.061 \cdot 10^4$.

The error bars shown in the diagram of Figure 2 are following the Gaussian error propagation:

$$\Delta I_r = \sqrt{\left(\frac{1}{r - b_r} \cdot \Delta g \right)^2 + \left(\frac{g - b_g}{(r - b_r)^2} \cdot \Delta r \right)^2 + \left(\frac{1}{r - b_r} \cdot \Delta b_g \right)^2 + \left(\frac{g - b_g}{(r - b_r)^2} \cdot \Delta b_r \right)^2} \tag{2}$$

where g is the averaged signal intensity at 550 nm, r is the averaged signal intensity at 700 nm, b_g is the averaged background signal intensity at 550 nm, b_r is the averaged background signal intensity at 700 nm and Δg, Δr, Δb_g and Δb_r are the standard deviations of respective values.

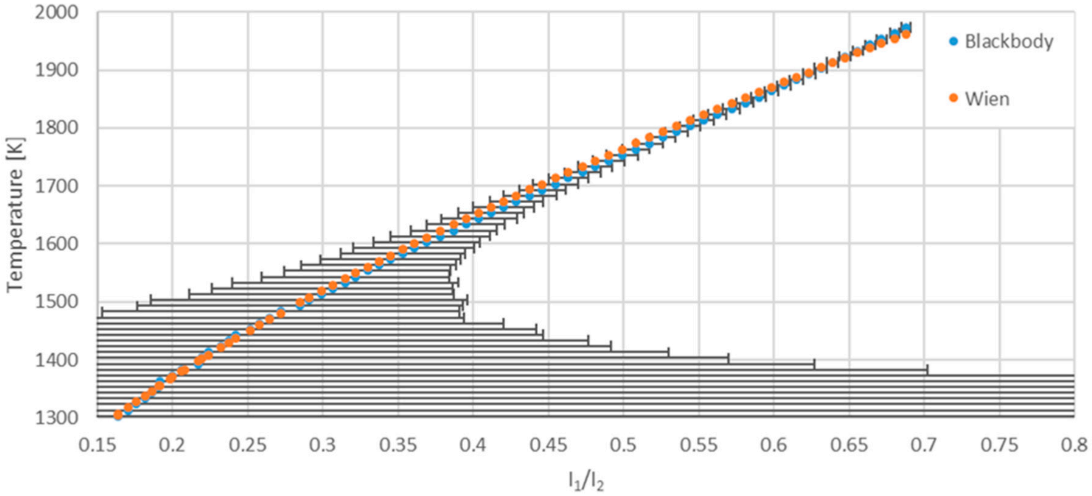

Figure 2. This figure shows the temperature calibration data from blackbody reference measurements and the fitted function data of Wien's law Equation (1).

Reliable temperature measurements resulting from Figure 2 can be performed down to temperatures of about 1550 K, even if the theoretical trend and the measured intensity ratios at low temperatures still fit well. At lower temperatures, signal intensities are to small (<1% of the intensity at maximum temperature) and the measurement uncertainties caused by the blackbody uncertainty rises dramatically compared to the intensity ratios. Additionally note, that particle size is still of crucial interest observing the particle temperature uncertainty. Large particles lead to higher signal intensities, which causes lower temperature uncertainty even at low temperatures.

2.2. Particle Emissivity Calculation

For emissivity calibration measurements, the IR-detector arm is placed in front of the blackbody. Precision pinholes of eight different diameters in the range of 50–600 µm, placed in front of the blackbody, simulate different sized particles. Again, for each pinhole diameter the temperature is varied in steps of 20 K from 1973.15 to 573.15 K. Three measurements, including 15,000 data points each for the InSb-detector and 50 spectrums at an integration time of 100 ms with the fiber spectrometer, are performed for each temperature/pinhole diameter combination. The background reduced and averaged InSb-data of each measurement lead to the temperature and diameter dependent reference signal intensity presented in Figure 3.

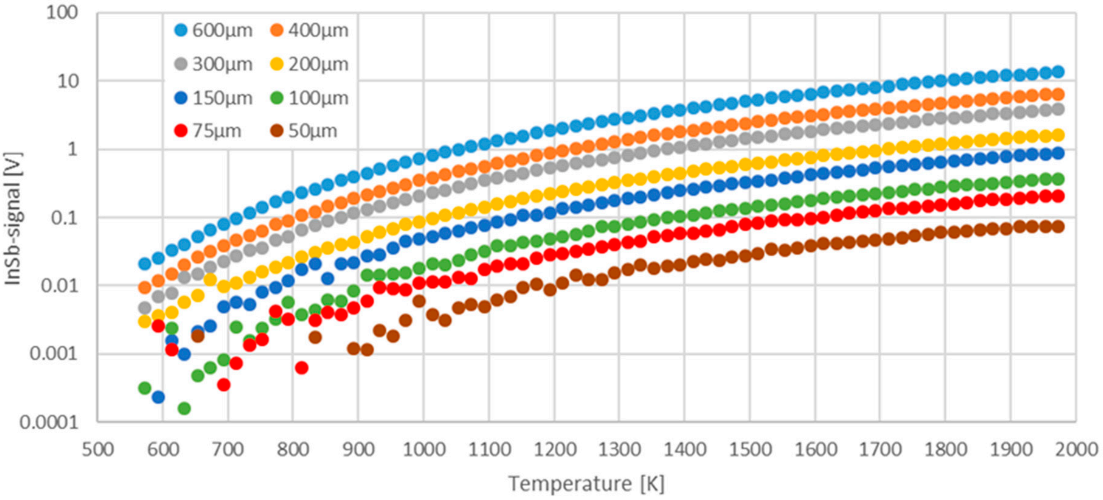

Figure 3. This figure shows the measured blackbody reference data.

To receive a three-dimensional set of reference data points including the temperature, the diameter and the intensity, the data for a constant temperature are fitted by the function:

$$I_b(d_b) = a \cdot (d_b)^b \tag{3}$$

where d_b denotes the pinhole diameter, exemplary presented in Figure 4a for 1400 K. The fitted curves lead to the three-dimensional reference set. In order to calculate the emissivity for particles with temperatures higher than 2000 K, this set needs to be extended. For every diameter between 50 µm and 800 µm the following function is fitted to the data:

$$I_b(T_b) = a \cdot (T_b)^b \tag{4}$$

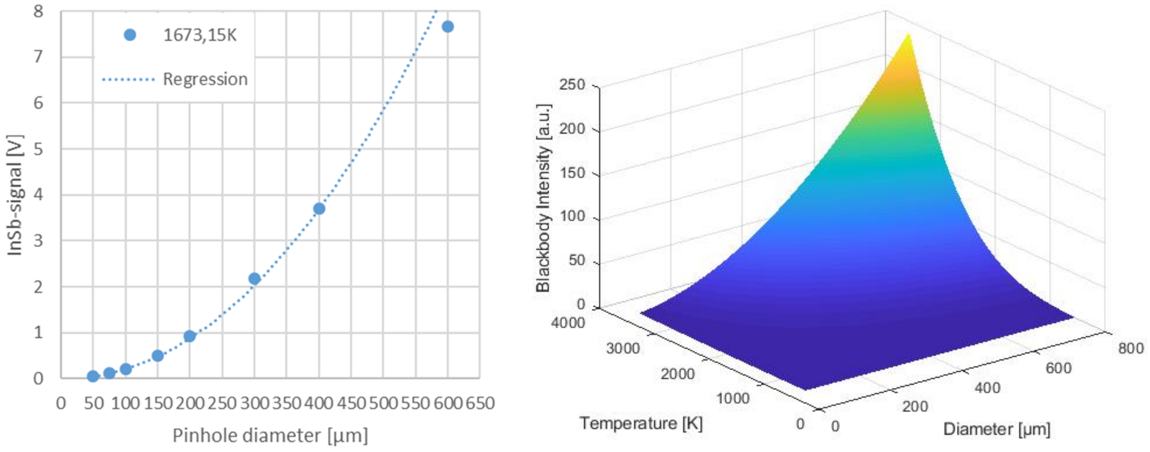

(**a**) (**b**)

Figure 4. This figure shows the measured blackbody reference data fitted by an exponential function exemplary for 1400 K (**a**) and an extended 3d surface (**b**) calculated from all reference data for all diameters between 50 µm and 800 µm and temperatures between 300 K and 3500 K.

By calculating all values resulting from these fits, the extended surface shown in Figure 4b results.

In both mesh calculations, parameter b of the fits is calculated as 2 in case of the diameter dependency and 4 in case of the temperature dependency. Obviously, these results are expected from general knowledge and underline the accuracy of the calibration.

The same procedure was applied for the spectrometer. Here, for every pinhole-temperature combination, intensities from 50 spectra are averaged for each wavelength. The received values are treated like a single InSb data point. This leads to a 4-dimensional set of reference data including the temperature, the diameter, the signal intensity and the observed wavelength.

3. Particle Measurements and Results

The observed nutshell particles have a diameter of 200–450 µm. As observed by Panahi et al. [14] biomass chars generated under high heating rates are typically cenospheric with a very thin carbon shell. This is why an average diameter of 325 µm is assumed for all measurements of nutshell particles and no significant shrinkage is assumed as the cenospheric shell structure fixes all carbon at a layer far from the structure's center. In case of coal particles, the average diameter is assumed as 180 µm caused by a diameter distribution from 160–200 µm. Here the diameter is also assumed as constant over a whole measurement. An example of measured photomultiplier and InSb-data of a coal particle measurement is presented in Figure 5a.

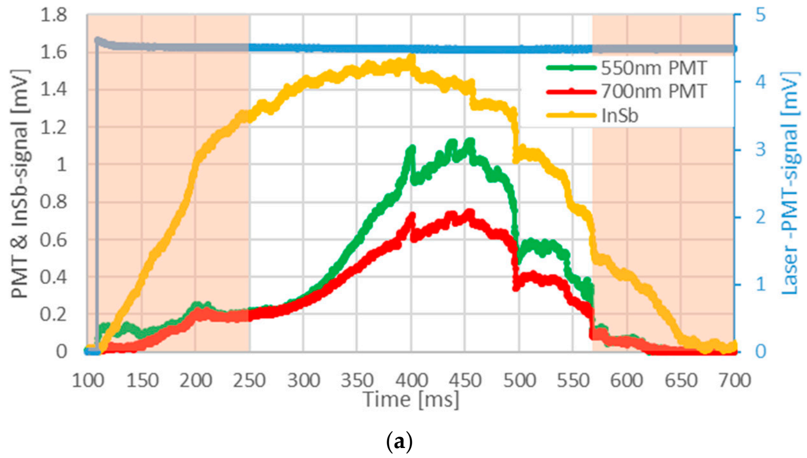

(**a**)

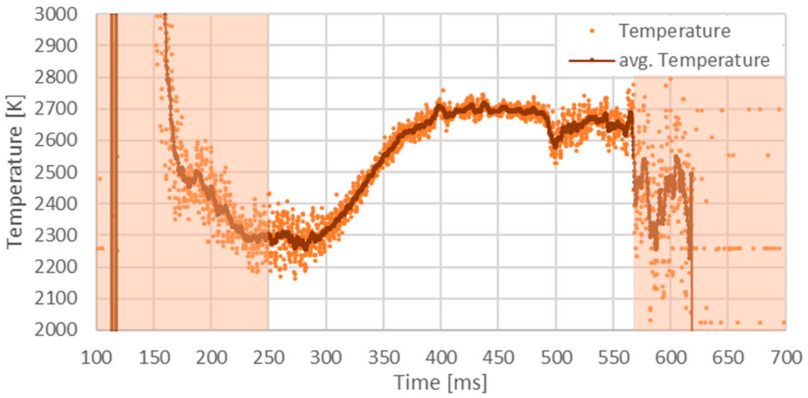

(**b**)

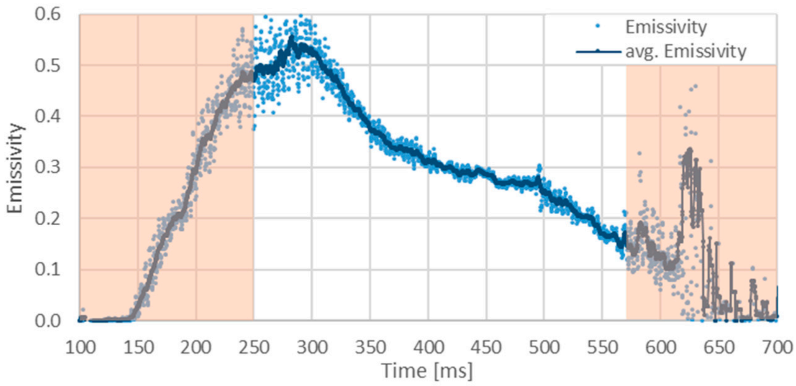

(**c**)

Figure 5. This figure shows an exemplary measured, time-resolved-measured photomultiplier and InSb-detector signals (**a**) and the corresponding calculated temperature (**b**) and emissivity (**c**) of a coal particle. Shaded regions are excluded from the data interpretation.

The corresponding temperature for each measured value is calculated using Equation (1). The time resolved temperature behavior is shown in Figure 5b. Depending on the temperature data, emissivity is determined:

$$\varepsilon = \frac{I_{p,}}{I_b} \tag{5}$$

where ε is the emissivity, I_p is the measured particle radiation intensity and I_b is the corresponding temperature and wavelength dependent calculated reference intensity from blackbody radiation.

An example for the resulting emissivity data is shown in Figure 5c. The averaged curves denoted in Figure 5b,c are calculated by a moving average of 20 values.

Laser ignition starts at about 110 ms and is constant over time, as a single particle is very likely to extinguish due to heat loss to the surroundings when no external heat source is available. The laser light leads to a direct rise of the 550 and 700 nm PMT signal to 0.15 mV for 550 nm and 0.05 mV for 700 nm. A suspected reason for this rise was laser light detected by the PMTs. This was excluded by test measurements. Placing a needle instead of a particle into the setup and performing a test measurement, the PMTs did not show any signals, even though laser radiation was visibly scattered into their direction. This leads to the reasonable assumption that the detected radiation in the beginning of the particle measurement must be emitted by the particle during devolatilization. During this process period, one cannot assume the particle as a gray radiator. A significant fraction of the thermal radiation is typically emitted by soot forming from volatile combustion. Determination of soot temperatures by ratio pyrometry would require further investigations and models, some of these being summarized in [15], furthermore, it is not the scope of current experiment. Therefore, the temperature measurements presented in the ignition phase are not reliable without further consideration of soot parameters and the radiation does not represent char optical properties. To avoid these effects, the data until 250 ms are neglected (marked red in Figure 5a–c). In the following, a period of 50 ms, where both curves rise equally, lead to a constant temperature of about 2300 K. From 300 ms to 400 ms, the temperature rises, as the 550 nm PMT-curve increases with a steeper slope than the 700 nm curve, up to 2700 K (note that the laser still heats the particle). From this point onwards, the temperature stays constant, even though both PMT-signals still rise. The two PMT graphs reach their maximum simultaneously at about 450 ms with the maximum values of 1.15 mV (550 nm) and 0.75 mV (700 nm). In the following, both curves decrease in three steps divided by two falling edges at 500 ms and 570 ms. These dips could be caused by particle movement and are observed in both PMTs. Even if they are not significantly influencing the 550 and 700 nm PMT-signal ratio, they cause a temperature drop of 100 K at 500 ms and a beginning temperature collapse at 570 ms. Additionally, in the end of the reaction, the PMT-signals are getting small. This leads to a worse signal to noise ratio and unreliable temperature data. For this reason, the data after 570 ms is neglected (marked red in Figure 5a–c).

The InSb-Signal also starts to rise with laser ignition. Until 200 ms there is a linear increase up to 1 mV followed by a peak at 400 ms and 1.6 mV. After the maximum is reached, the curve decreases in the same stepwise behavior like the PMT graphs.

The resulting emissivity in the reliable range shows a small rise in the beginning (250–300 ms) with a maximum of 0.55 followed by a continuously decreasing behavior from 300–570 ms to 0.15. Comparing this to the temperature behavior, one can observe the decreasing emissivity at rising temperature. This fits to the expectations caused by the work of Greaser et al. [11].

Temperature Dependent Emissivity Evaluation

Following the same method, the measurements of a total of five different coal particles and six nutshell particles were analyzed. For each particle, the temperature, emissivity combinations are divided into temperature classes of 100 K from 1950–3650 K. In the next step, the data from all particles belonging to one fuel are combined for each temperature class, which adds information on particle-to-particle variations. As a result, as the high readout frequency of the InSb and the PMTs provides a large number of data points for averaging, each temperature class contains at least 15 separate emissivity values after this temperature binning and particle averaging. Figure 6 presents the resulting temperature-dependent emissivity of nutshell and coal particles, denoting that for every temperature class emissivity values from at least three different particle measurements were needed to accept the average value as reliable. Data points of the resulting temperature range edges (below 2250 K for coal and 2050 K for nutshell and over 3450 K for coal and 2950 K for nutshell), including only data from two or a single particle measurement, are neglected.

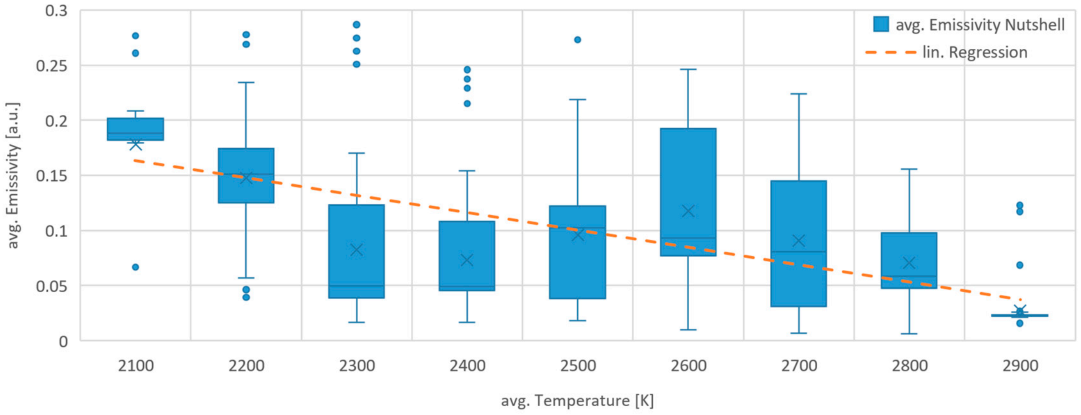

(**a**)

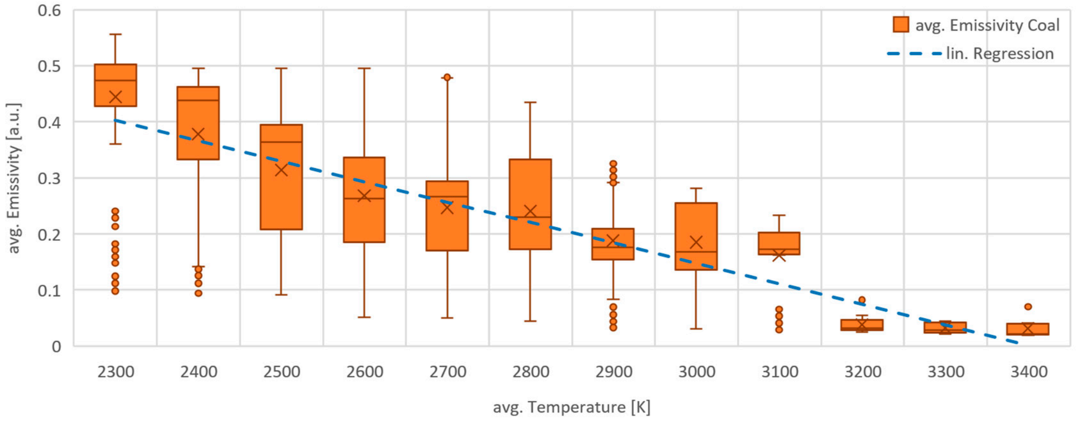

(**b**)

Figure 6. This figure summarizes temperature-dependent averaged emissivity of multiple nutshell (**a**) and coal particles (**b**).

For both fuels the curves show a decreasing trend with rising temperature. Observing the class averages, marked with a cross, for the nutshell in Figure 6a, emissivity starts at a value of about 0.18 at 2100 K, decreases to a local minimum of 0.075 at 2400 K, rises to a local maximum of 0.12 at 2600 K and decreases again to the global minimum of 0.03 at 2900 K. Even though this behavior shows no clear trend in the first impression, looking at the value distribution for every temperature class, the effect of a decreasing emissivity at higher temperatures gets more visible. In the temperature range from 2300–2800 K the number of values between the 1st and 3rd quartile is always over 180 values. This causes a wider distribution and, therefore, a more visible trend, especially at the local maximum at 2600 K, where the range between the 1st quartile and the median is very small compared to the other sections in this class. In contrast to this, the other classes include just 30 to 53 different values, which causes narrower distributions. Compared to the nutshell data, the coal data shown in Figure 6b decreases almost constantly from 0.45 at 2300 K to 0.03 at 3400 K. The plot shows a value distribution range between the 1st and 3rd quartile of 0.05 and 0.2 in the range of 2300–3000 K. For higher temperatures, this range gets smaller and is in the range from 0.4 to 0.2. This effect is caused by the number of values included in the specific temperature classes. The classes from 2300–3000 K include over 500 values each, whereas the other classes consist of 15 to 310 values. Also the averages show a more clear trend of a decreasing emissivity at increasing temperatures. Additionally, it is clearly visible, that the nutshell emissivity is much lower than the coal emissivity and the coal in this setup burns at slightly higher temperatures than the nutshells.

To get an overall impression of the emissivity behavior of both fuels, linear regressions of the averaged were calculated. The linear regression for both average value curves is chosen in accordance to temperature-dependent emissivity correlation in [12]. Although these linear correlations are not based on any particular theory, the regression parameters, $R^2 = 0.784$ in case of nutshells and $R^2 = 0.956$ in case of coal, provide the best fit. The two linear regression functions for nutshell and for coal are as follows:

$$F_{nutshell}\left(T_p\right) = -1.5751 \cdot 10^{-4} \cdot T_p + 0.4949 \tag{6}$$

$$F_{coal}\left(T_p\right) = -3.6196 \cdot 10^{-4} \cdot T_p + 1.2424 \tag{7}$$

The decreasing emissivity of fuel particles at increasing temperatures fits to the expected behavior from the literature [12,16,17]. Although there are slight local minima and maxima in the emissivity of both fuels, the trend is clearly shown. For the coal particles, the received emissivity data enlarge the former known data of Graeser et al. shown in Figure 7.

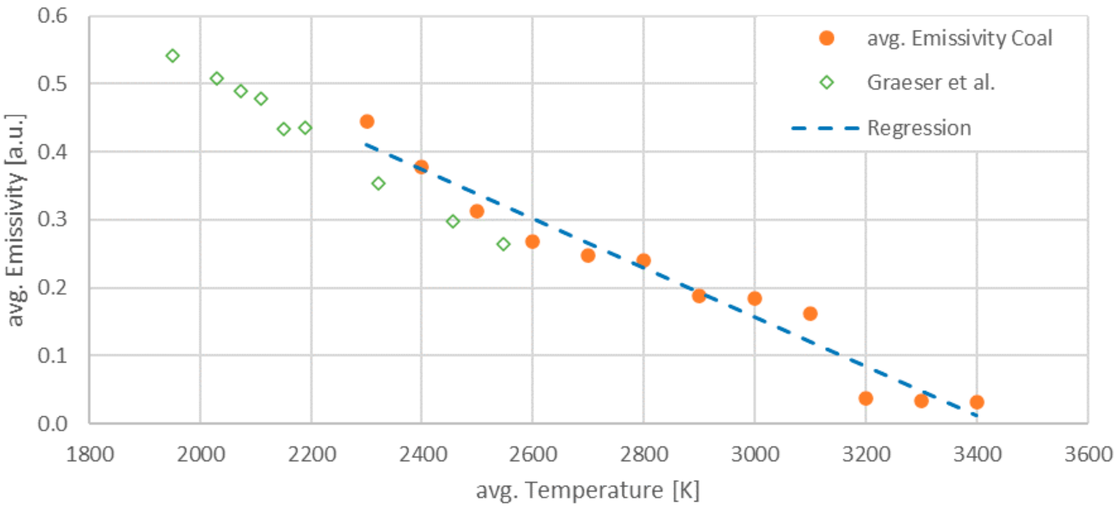

Figure 7. This figure shows the temperature-dependent averaged emissivity of coal particles observed in this work added by literature data from Graeser et al. [11].

Even if the number of observed particles in this work is still low and needs to be increased in future measurements, the trend and the region of the received emissivity data follows the values Graeser et al. [11] measured. The agreement between both curves is remarkable. As the same detectors (PMTs and InSb) have been used for this work and Graeser et al. [9] and the coal samples are quite similar for both data sets, this agreement is not very surprising. The temperature-dependent box plots from Figure 6 give an impression on the statistical scatter in the data, which needs to be considered for this correlation. Globally, for all temperatures an uncertainty in the range of $\Delta\varepsilon \sim 0.2$ seems to be justifiable. This is in agreement with the scatter from most of the other publications dealing with pulverized fuel emissivity [10,11,13].

4. Conclusions

In the current work, a setup for particle emissivity measurements and its calibration process is presented. Using a blackbody reference radiation source, particle temperature and emitted radiation between 2.4–5.5 µm can be determined. The emissivity of observed nutshell and coal particles is decreasing at increasing temperature, which fits to the literature data base. The emissivity of nutshell particles decreases from 0.18 at 2300 K to 0.03 at 2900 K. The emissivity of coal particles decreases linearly from 0.45 at 2300 K to 0.03 at 3400 K. The emissivity of nutshell particles is always lower than the one of coal, at equal temperature. This indicates the emissivity to be dependent on the fuel rank. So far, there are no systematic descriptions of this connection but offer a need in further investigations.

Additionally, the coal particle emissivity data fit the ones from the literature and enlarge the range of existing data.

Author Contributions: Conceptualization, L.P. and M.S.; methodology, L.P. and M.S.; software, L.P. and Y.G.; validation, L.P. and Y.G.; formal analysis, L.P. and Y.G.; investigation, L.P.; resources, L.P.; data curation, L.P.; writing—original draft preparation, L.P.; writing—review and editing, M.S. and Y.G.; visualization, L.P.; supervision, M.S.; project administration, L.P. All authors have read and agreed to the published version of the manuscript.

Funding: This work was funded by the German Research Foundation (DFG) within the framework of the SFB/ Transregio 129 ''Oxyflame". Gefördert durch die Deutsche Forschungsgemeinschaft (DFG)—Projektnummer 215035359—TRR 129.

Acknowledgments: We acknowledge support by the DFG Open Access Publication Funds of the Ruhr-Universität Bochum.

Conflicts of Interest: The authors declare no conflict of interest. The funders had no role in the design of the study; in the collection, analyses, or interpretation of data; in the writing of the manuscript, or in the decision to publish the results.

References

1. Yin, C. On gas and particle radiation in pulverized fuel combustion furnaces. *Appl. Energy* **2015**, *157*, 554–561. [CrossRef]
2. Johansson, R.; Leckner, B.; Andersson, K.; Johnsson, F. Influence of particle and gas radiation in oxy-fuel combustion. *Int. J. Heat Mass Transf.* **2013**, *65*, 143–152. [CrossRef]
3. Chen, W.-H.; Cheng, W.-Y.; Lu, K.-M.; Huang, Y.-P. An evaluation on improvement of pulverized biomass property for solid fuel through torrefaction. *Appl. Energy* **2011**, *88*, 3636–3644. [CrossRef]
4. Gronarz, T.; Schulze, J.; Laemmerhold, M.; Graeser, P.; Gorewoda, J.; Kez, V.; Habermehl, M.; Schiemann, M.; Ströhle, J.; Epple, B.; et al. Quantification of the influence of parameters determining radiative heat transfer in an oxy-fuel operated boiler. *Fuel Process. Technol.* **2017**, *157*, 76–89. [CrossRef]
5. Murphy, J.J.; Shaddix, C.R. Combustion kinetics of coal chars in oxygen-enriched environments. *Combust. Flame* **2006**, *144*, 710–729. [CrossRef]
6. Mitchell, R.E. Experimentally determined overall burning rates of coal chars. *Combust. Sci. Technol.* **1987**, *53*, 165–186. [CrossRef]
7. Schiemann, M.; Geier, M.; Shaddix, C.R.; Vorobiev, N.; Scherer, V. Determination of char combustion kinetics parameters: Comparison of point detector and imaging-based particle-sizing pyrometry. *Rev. Sci. Instrum.* **2014**, *85*, 075114. [CrossRef] [PubMed]
8. Meesri, C.; Moghtaderi, B. Experimental and numerical analysis of sawdust-char combustion reactivity in a drop tube reactor. *Combust. Sci. Technol.* **2003**, *175*, 793–823. [CrossRef]
9. Tchapda, A.H.; Pisupati, S.V. Characterization of an entrained flow reactor for pyrolysis of coal and biomass at higher temperatures. *Fuel* **2015**, *156*, 254–266. [CrossRef]
10. Graeser, P.; Schiemann, M. Emissivity of burning bituminous coal char particles—Burnout effects. *Fuel* **2017**, *196*, 336–343. [CrossRef]
11. Graeser, P.; Schiemann, M. Investigations on the emissivity of burning coal char particles: Influence of particle temperature and composition of reaction atmosphere. *Fuel* **2020**, *263*, 116714. [CrossRef]
12. Schiemann, M.; Gronarz, T.; Graeser, P.; Gorewoda, J.; Kneer, R.; Scherer, V. A correlation between char emissivity and temperature. *Fuel* **2019**, *256*, 115889. [CrossRef]
13. Graeser, P.; Schiemann, M. Char particle emissivity of two coal chars in oxy-fuel atmospheres. *Fuel* **2016**, *183*, 405–413. [CrossRef]
14. Panahi, A.; Vorobiev, N.; Schiemann, M.; Tarakcioglu, M.; Delichatsios, M.; Levendis, Y.A. Combustion details of raw and torrefied biomass fuel particles with individually-observed size, shape and mass. *Combust. Flame* **2019**, *207*, 327–341. [CrossRef]
15. Khatami, R.; Levendis, Y.A.; Delichatsios, M.A. Soot loading, temperature and size of single coal particle envelope flames in conventional- and oxy-combustion conditions (O2/N2 and O2/CO2). *Combust. Flame* **2015**, *162*, 2508–2517. [CrossRef]

16. Greffrath, F.; Gorewoda, J.; Schiemann, M.; Scherer, V. Influence of chemical composition and physical structure on normal radiant emittance characteristics of ash deposits. *Fuel* **2014**, *134*, 307–314. [CrossRef]
17. Gorewoda, J.; Scherer, V. Influence of carbonate decomposition on normal spectral radiative emittance in the context of oxyfuel combustion. *Energy Fuels* **2016**, *30*, 9752–9760. [CrossRef]